Direct Growth of Lateral ZnO Nanorod UV Photodetectors with Schottky Contact by a Single-Step Hydrothermal Reaction

Nishuang Liu,[†] Guojia Fang,[*,†,‡] Wei Zeng,[†] Hai Zhou,[†] Fei Cheng,[†] Qiao Zheng,[†] Longyan Yuan,[†] Xiao Zou,[†] and Xingzhong Zhao[†]

Key Laboratory of Artificial Micro- and Nano-structures of Ministry of Education, Department of Electronic Science and Technology, School of Physics and Technology, Wuhan University, Wuhan 430072, P. R. China, and State Key Laboratory of Transducer Technology, Chinese Academy of Sciences, Shanghai, 200050, P. R. China

ABSTRACT Lateral zinc oxide (ZnO) nanorod metal-semiconductor-metal ultraviolet detectors with different metal contact were fabricated on glass substrate by a single-step hydrothermal reaction. With the combined effect from a ZnO seed layer and an inactive layer for nanorod growth, ZnO nanorods could grow laterally and aligned between the interdigitated electrodes. When the growth process is terminated, the integration of ZnO nanorods into a function device can be achieved in the meantime. The structure can be modeled as being composed of two same Schottky barriers connected back to back, in series with a resistance of R. The devices are visible-blind and have great response even in mid ultraviolet region. The photodetectors with Ni electrode show better performance both in the aspect of photocurrent and response time, owing to the larger Schottky barrier at the Ni/ZnO interface. By surface coating with polymethyl methacrylate, the response has been further improved. Our approach provides a simple and effective way to fabricate high performance ultraviolet detectors.

KEYWORDS: direct growth • ZnO nanorods • hydrothermal reaction • UV photodetector • Schottky contact

1. INTRODUCTION

Zinc oxide (ZnO) is an attractive wide direct band gap (3.37 eV at room temperature) oxide semiconductor with a large exciton binding energy of 60 meV, which makes it suitable for fabrication of ultraviolet (UV) photodetectors (PDs), and UV light emitting devices (1, 2). Moreover, one-dimensional ZnO nanostructures are especially attractive because of their unique properties such as high surface-to-volume ratio and carrier confinement in two dimensions that could improve device performance. However, how to put the nanostructures into devices is still a challenge. The most popular choice is the conventional "pick and place" method. In this way, nanostructures are flaked away from their initially grown substrates, and then are dispersed randomly on an insulating substrate. At last, sophisticated techniques such as electron beam lithography (3) or focused ion beam (4) are required to make metallic contacts to the nanostructures. Although this way offers a means to put nanomaterials into working device, it is time-consuming and complicated, which blocks its way to practical applications. Recently, another technique based on bridging growth of nanowires has been developed and shows promising properties (5–7). In this technique, a channel is etched into a single-crystal substrate and nanostructures are grown across the channel from one side to the other. Therefore, the device fabrication process is much more efficient compared to the conventional "pick and place" way. However, microfabrication techniques such as wet etching and reactive ion-etching are still needed to make the channel, which make this method still not easy enough for practical applications. Therefore, much research has been carried out worldwide to find a better method (8–10).

In this paper, we demonstrate a ZnO bridging nanorod metal-semiconductor-metal (MSM) UV detector fabricated on glass substrate by a single-step hydrothermal reaction. It has been reported that some materials can inhibit the growth of ZnO nanorods (11–13). With this mechanism, we can achieve the laterally aligned growth of ZnO nanorod arrays using the combined effect from ZnO seed layer and catalytically inactive layers. Moreover, we used different metal contacts, modified the ZnO nanorods with polymethyl methacrylate (PMMA) films, and measured the effect on the photoresponse characteristics. The photoresponse mechanism is accordingly analyzed and discussed.

2. EXPERIMENTAL SECTION

Before growing the ZnO nanorods, a 300 nm ZnO seed layer was deposited on the glass substrate using a radio frequency magnetron sputtering deposition system. To prepare interdigitated electrode patterns, a conventional photolithography followed by lift-off techniques was used. We then sputtered different metal (Sn and Ni) layer on the patterned ZnO seed layer for preventing the local growth of ZnO and serving as metal contacts in the meantime. The fingers of the contact electrodes were 100 μm long and 5 μm wide with 5 μm spacing. The active area of the whole device was 100 × 100 μm^2. The

* To whom correspondence should be addressed. Tel: +86 (0)27 68752147. Fax: +86 (0)27 68752569. E-mail: gjfang@whu.edu.cn.
Received for review March 29, 2010 and accepted June 7, 2010
† Wuhan University.
‡ Chinese Academy of Sciences.
DOI: 10.1021/am100277q

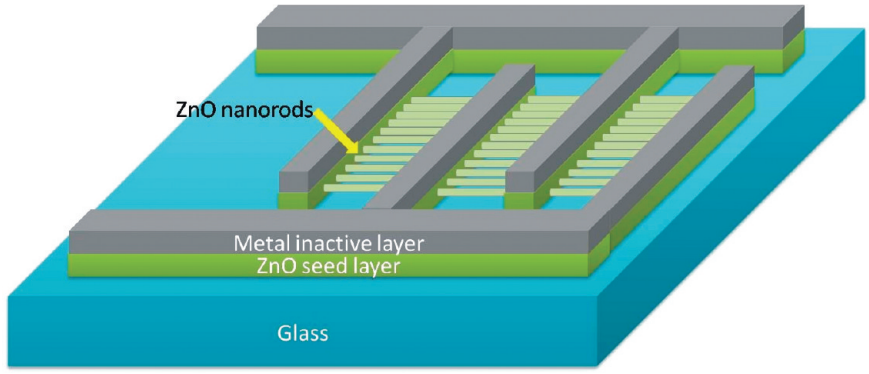

FIGURE 1. Schematic diagram for the fabricated UV photosensor with laterally aligned ZnO nanorods.

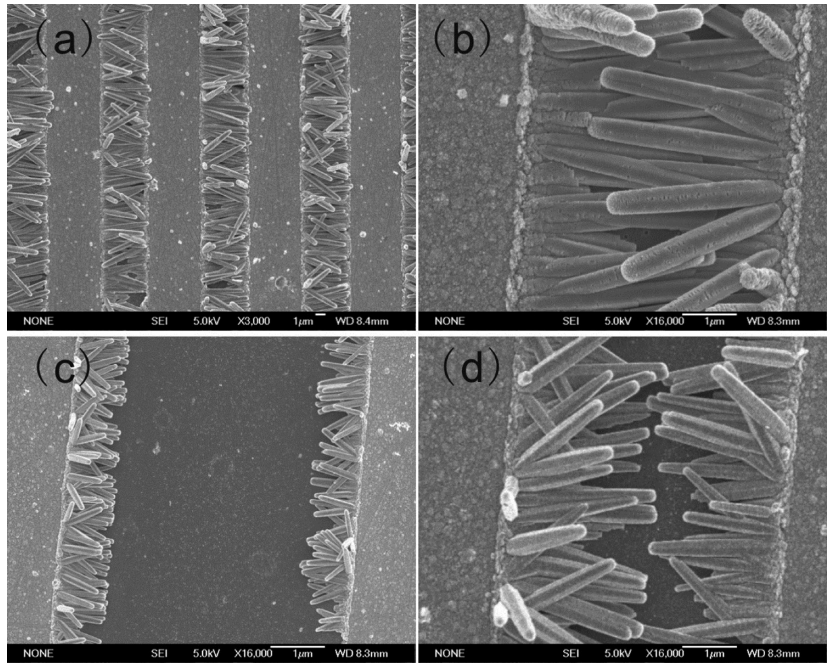

FIGURE 2. (a, b) FESEM images of a typical ZnO nanorods PD with different magnification. FESEM images of two samples with different reaction time of (c) 30 min and (d) 1 h.

nutrient solution for ZnO nanorods growth was an aqueous solution of 2 mM zinc nitrate [$Zn(NO3)_2 \cdot 6H_2O$] and hexamethylenetetramine. The reaction was kept at 90 °C for 2 h. The fabricated MSM PDs were removed from the solution, rinsed with distilled water, and dried in air. Finally, some of them were modified with a 520 nm thick PMMA layer by spin coating. Figure 1 shows the schematic structure of the proposed ZnO nanorod MSM PD.

The morphology of the as-grown ZnO nanorod arrays was characterized by field emission scanning electron microscopy (FESEM, FEI XL-30). Photoluminescence (PL) and high-resolution transmission electron microscopy (HRTEM JEOL JEM 2010) were then used to characterize the optical and crystallographic properties of the as-grown ZnO nanorods. A Keithley 4200 semiconductor parameter analyzer was then used to measure current−voltage ($I-V$) characteristics of the fabricated ZnO nanorod PDs. Spectral responsivity measurements were also performed with a mercury arc lamp light source and a standard synchronous detection scheme. All of the measurements were carried out at room temperature in ambient condition.

3. RESULTS AND DISCUSSION

Images a and b in Figure 2 show the physical structure of a typical ZnO nanorods PD. It can be seen that ZnO nanorods grew laterally between the interdigitated electrodes with a good alignment. Owing to the covered metal inactive layer, more than 80% of the ZnO nanorods are parallel to the substrate. From Figure 2b, we can observe that ZnO nanorods have a diameter about 300 nm and a length of about 4 μm. And the hexagonal cross-section of nanorods implies that c axis of ZnO nanorods is along its length direction. The position controlled growth of the nanorods implies that the nucleation leading to the growth of nanorods takes place only at the open area exposed to the edge of ZnO seed layer. Moreover, by tuning the reaction time and the gap between two electrodes, we can control the physical structure of the ZnO nanorods PD more accurately. For example, as shown in images c and d in Figure 2, there are two samples with reaction time of 30 min and 1 h, respectively. As we can see from the FESEM images, ZnO nanorods grew longer along horizontal direction with increasing reaction time. Especially, the ZnO nanorods from two sides almost connected to each other, as shown in Figure 2d. It indicates the possibility that we can achieve some nanogap devices through this method.

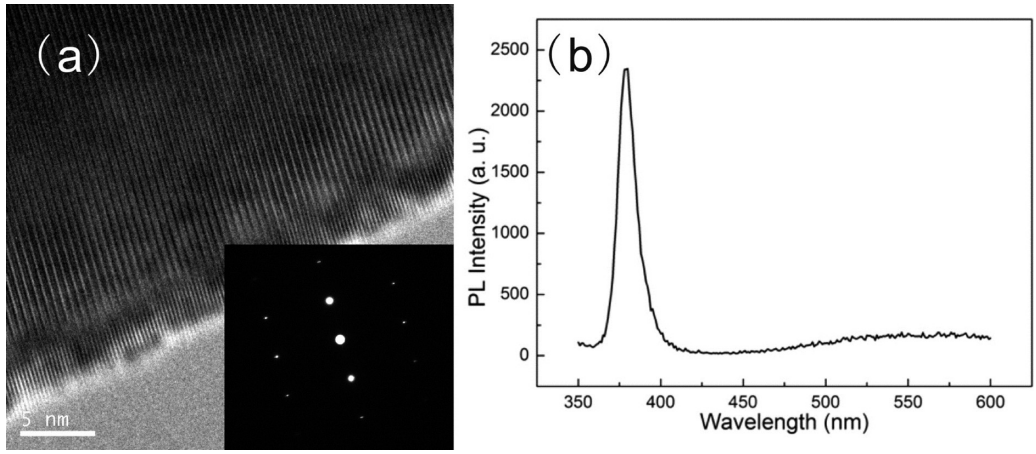

FIGURE 3. (a) HRTEM picture of a single ZnO nanorod. (b) Room temperature PL spectrum of ZnO nanorods.

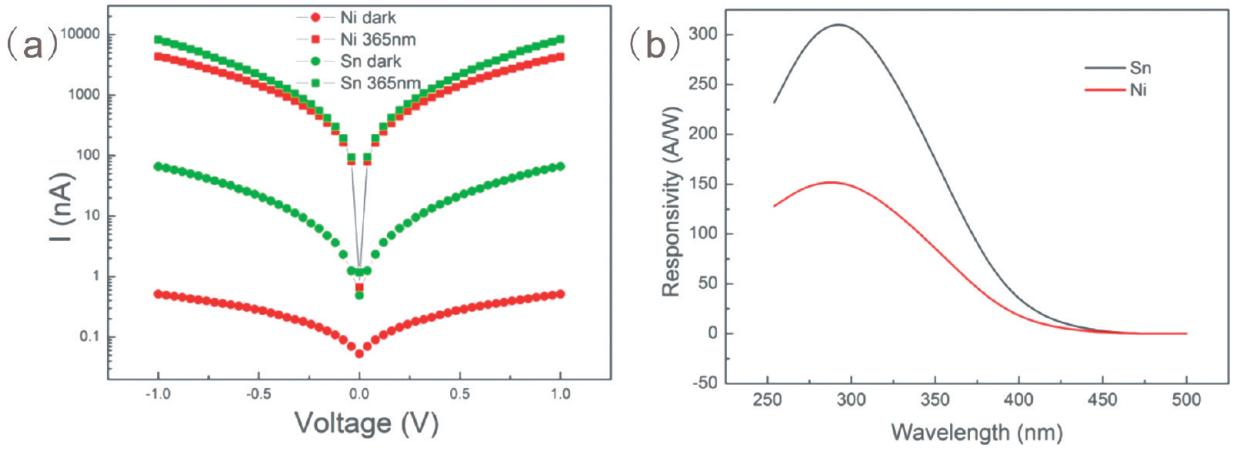

FIGURE 4. (a) $I-V$ characteristics of the ZnO nanorod PDs with different metal electrodes measured in dark and under 365 nm illumination. (b) Measured spectral responsivities of the ZnO nanorod PDs with Sn and Ni electrodes.

The detailed structural characterization of the as-grown ZnO nanorod is performed by HRTEM. The HRTEM image and selective area electron diffraction (SAED) pattern (Figure 3a) indicate that the ZnO nanorods are structurally uniform and contain no defects such as dislocations or stacking. The lattices spacing of 0.52 nm corresponds to a *d*-spacing of (002) crystal planes, indicating growth of the crystalline ZnO nanorods is along the *c*-axis direction. Figure 3b illustrates the PL spectrum of the ZnO nanorods excited by a 325 nm He−Cd laser at room temperature. It can be seen that the as-grown ZnO nanorods have a sharp UV emission at 380 nm and a broad much suppressed deep level visible emission at 580 nm. We can observe that the full width at half-maximum (fwhm) value of UV peak of the as-grown ZnO nanorods is ∼13 nm. It should be accented that the weak emission in the visible region is almost negligible. The sharp and intense UV emission corresponding to the near band-edge emission is normally attributed to the exciton recombination (14, 15). The deep-level transition is related to the oxygen vacancies, surface states, and some structural defects (16). Therefore, this visible emission resulted from the radiative recombination of a photogenerated hole with an electron occupying the oxygen vacancies (15). The relative PL intensity ratio of the UV near-band-edge emission to deep-level emission is related to the crystal quality of ZnO nanostructures (17).

Figure 4a shows typical current−voltage ($I-V$) characteristics of the fabricated ZnO nanorod MSM PDs with Sn and Ni electrodes measured in dark and under 0.11 mW/cm^2 UV light illumination ($\lambda = 365$ nm). With 1 V bias voltage, the photocurrent to dark current contrast ratios of the ZnO nanorod PDs with Sn electrode and Ni electrode were 125 and 8380, respectively. The origin of more photocurrents generated from the ZnO nanorods PD with Ni electrode will be discussed in the later part of this paper. Figure 4b shows the spectral responsivities of ZnO nanorod PDs with 1 V applied bias. The responsivity of the fabricated ZnO nanorod PDs with Sn and Ni electrode under illumination of 365 nm were 120 and 61 A/W, respectively. The UV/visible rejection ratio can be defined as the responsivity at 365 nm divided by that at 450 nm. And it was about 1906 for the device with Ni electrode, indicating that the ZnO nanorod device exhibits relatively high signal-to-noise ratio. Meanwhile, the ZnO nanorod devices are visible-blind and have relative high response even in the mid-UV region, as shown in Figure 4b. Moreover, photoconductive gain (G) is defined as the ratio of the number of electrons collected per unit time (N_{el}) to

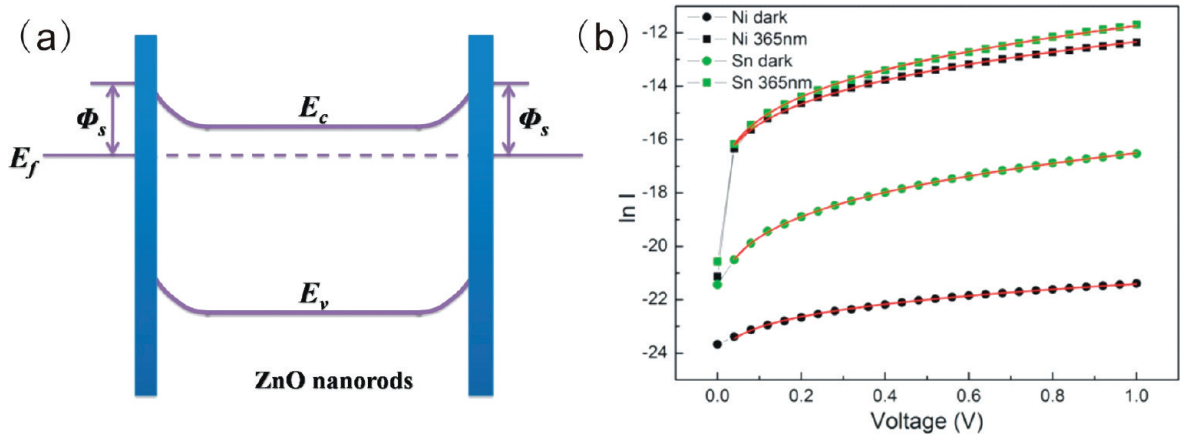

FIGURE 5. (a) Schematic band diagram showing band bending at the metal semiconductor contacts with no applied voltage. (b) Fitting the ln $I-V$ data of the devices with Sn and Ni electrodes in dark and under UV illumination using the thermionic emission-diffusion theory. The red lines are the theoretical fit of ln $I-V^{1/4}$.

the number of absorbed photons per unit time (N_{ph}); this ratio can be derived as (3)

$$G = \frac{N_{el}}{N_{ph}} = R\frac{1.24}{\lambda(\mu m)}\frac{1}{\eta} = \frac{\tau}{\tau_{tr}} = \frac{I_{ph}}{qF} \quad (1)$$

where R is the responsivity of a detector, λ is incident light wavelength, η is quantum efficiency, τ is hole (minority) lifetime, τ_{tr} is electron transit time, I_{ph} is photocurrent, q is the elementary charge, and F is photo absorption rate. By applying 120, 61 A/W, and 365 nm to the expression, the gain of the ZnO nanorod PDs with Sn and Ni electrodes are estimated to be 407 and 207 by assuming $\eta = 1$ just for simplicity (18). It may suggest that the ZnO nanorod PDs all have internal gain.

Moreover, the $I-V$ curves of the ZnO nanorod PDs exhibited almost symmetrical nonlinear behaviors, which have been reported in many literature reports (19, 20). The nonlinear behaviors is caused by the Schottky barriers (SB) formd between the semiconductor and the metal electrodes, and the shape of $I-V$ curves depends on the heights of the Schottky barriers at the interface of metal and semiconductor. So the almost symmetrical $I-V$ curves mean that the two Schottky barriers height are at almost the same value. Generally, metal Ni (work function of 5.15 eV) and n-type ZnO (work function of 5.1 eV) can form a Schottky contact. In our experiment, the Sn (work function of 4.3 eV) electrode also forms a Schottky contact with ZnO nanorods. In fact, the similar nonlinear $I-V$ characteristics are commonly observed in measuring semiconductor devices (19, 20). Anyway, the MSM structure in our experiment can be modeled as being composed of two Schottky barriers with the same height connected back to back, in series with a semiconductor having a resistance R (19, 20), as shown in Figure 5a. At a fixed applied bias V, the voltage drops occurs main at the reversely biased Schottky barrier ϕ_s (eV), and it is denoted by V_s. Because the voltage at the forward biased Schottky barrier is almost neglectable, we assume $V_s \approx V$. Considering that our devices all worked at room temperature and the ZnO nanorods had a low doping, we believe that the dominant transport property at the barrier is thermionic emission and diffusion, while the contribution of tunneling can be ignored (21, 22). Therefore, in our experiment, the current through the reverse bias Schottky barrier is as follows based on classic thermionic emission-diffusion theory (21) (for $V \gg 3kT/q \approx 77$ mV)

$$I = SA^{**}T^2\exp\left(-\frac{\phi_s}{kT}\right) \times \exp\left(\frac{\sqrt[4]{q^7 N_D(V + V_{bi} - kT/q)/8\pi^2\varepsilon_s^3}}{kT}\right) \quad (2)$$

where S is the area of the Schottky barrier, A^{**} is the effective Richardson constant, q is the electron charge, k is the Bolzman constant, N_D is the donor impurity density, V_{bi} is the build in potential at the barrier, and ε_s is the permittivity of ZnO. The ln $I-V$ curves shown in Figure 5b qualitative indicates that variation of ln I has a linear relationship with $V^{1/4}$ for reverse biased Schottky barrier instead of with V as for forward biased Schottky barrier. Therefore, eq 2 can be used to precisely fit the experimentally observed ln $I-V$ curve, from which the corresponding parameters can be derived. This indicates that the thermionic emission–diffusion model not only is the dominant process in our device but also can be applied to derive the SB height (22) as described in the following section.

By assuming that S, A^{**}, T, and N_D are constant, ϕ_s can, in principle, be derived from the logarithm of current (ln $I-V$) plot, which is shown in Figure 4b. Although it is hard to calculate the real value of Schottky barrier height ϕ_s, we can get the relative change of SB height all the same. Thus, the relative change of SB height can be determined by

$$\ln[I_1/I_0] = -\Delta\phi_s/kT \quad (3)$$

If we define the SB height of the ZnO nanorod device with Ni electrode at a value of x in dark, then we can obtain the change of SB height with Sn electrode in dark via the $I-V$ curves shown in figure. Finally SB height of the device with

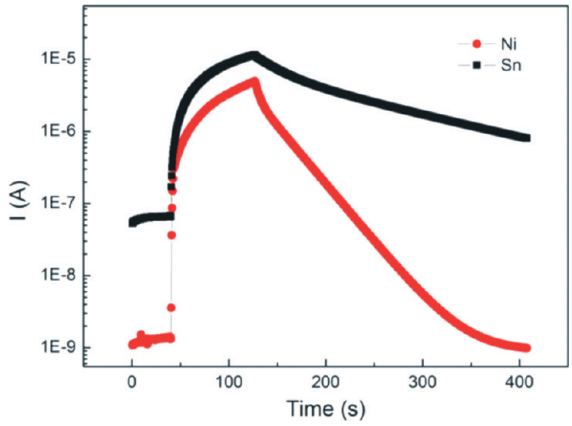

FIGURE 6. UV response time performance of the ZnO nanorods with Sn and Ni electrodes.

Sn electrode in dark is calculated to be *x*-125.8 meV at the biased voltage of 1 V. We also notice that the change of SB height is not very sensitive to the choice of bias voltage *V*. Considering the value of N_D is not a constant under UV illumination, we have not calculated the change of SB height under UV illumination via this means here.

Another important parameter for UV photodector is response time. Figure 6 shows the time-resolved photocurrent of the two ZnO nanorod PDs in response to the turn-on and turn-off of 0.11 mW/cm^2 UV illumination ($\lambda = 365$ nm). With the UV illumination on, the current of the ZnO PD with Ni electrode rises from 0.5 to 320 nA within 3 s. The rapid photocurrent raise is followed by a slower component, which follows to an exponential relation with a time constant of 452 s for the device with Ni electrode. It is generally accepted that oxygen molecules are adsorbed onto the ZnO surfaces by capturing free electrons from the n-type ZnO surface, where a low conductive depletion layer will be formed near the surface. The electron−hole pairs are photogenerated, while the photon energy of illumination exceeds band energy, which is about 3.37 eV for ZnO. This process is fast and responsible for the rapid rise of current in the first few seconds. The holes migrate to the surface because of the built-in potential produced by band-bending, and then discharge the negatively charged adsorbed oxygen ions. So oxygen is desorbed from the surface. The width of the depletion layer then decreases, and meanwhile, the flowing current increases (4, 9, 18). This process is slow and responsible for the following slower rise of current in the next stage. On the other hand, the decay processes are excellently fitted with a biexponential relaxation equation of the following type

$$I = I_0 + Ae^{-t/\tau_1} + Be^{-t/\tau_2} \quad (4)$$

where τ_1 and τ_2 are two relaxation time constants ($\tau_1 = 4.9$ s, $\tau_2 = 27.9$ s for the device with Ni electrode; $\tau_1 = 27.1$ s, $\tau_2 = 131.2$ s for the device with Sn electrode). Two time constants indicated that two different mechanisms are functioning during the decay processes, which have been reported in many literature reports about metal oxides (23, 24). The first one is a fast band-to-band recombination in their bulk with small characteristic times. The second one, which becomes dominant in nanoscale materials, is highly dependent on the existence of chemisorbed oxygen molecules at their surfaces, because holes discharge oxygen species from the surface by indirect electron−hole recombination mechanisms. This process has a much larger time constant. When the UV illumination is off, the two mechanisms both contribute to the recovery of the current. Prades et al. believe that the built-in potential in the nanorods near the surface caused by oxygen adsorption blocks the recombination of a part of the photogenerated electron−hole pairs, because holes are accumulated to the outer shell of the nanorods and electrons remain in the inner part (25). We believe this mechanism is responsible for the persistent photoconductivity phenomenon that exists in our experiment, as shown in Figure 6.

From Figure 6, we can find out that the ZnO nanorod PD with Ni electrode performs better both in the aspect of photocurrent and response time. We believe this phenomenon must be attributed to the Schottky contact at the ZnO/metal interface, which have been reported in recent literature (4, 26). As we described in the frontal part, the SB height of the device with Ni electrode is higher than the device with Sn electrode for about 125.8 meV, which results in a much smaller current as shown in the *I*−*V* characteristics of Figure 4a. The presence of a SB at the metal/ZnO interface plays a crucial role in the electrical transport performance of the MSM structure (21). Differences in performance between device with Ni electrode and device with Sn electrode can therefore be attributed to the effect of a higher injection barrier at the Ni/ZnO interface that blocks the charge injection. As shown in Figure 4a, the dark current with Sn electrode is 2 orders of scale larger than that with Ni electrode. Meanwhile, the photocurrent is also increased. It means that the injection barrier at the ZnO/metal interface controls the current, either in the dark or under illumination. So the photocurrent must arise partly from changes in the injection process. When the device with a SB is illuminated by 365 nm UV, photogenerated electrons and holes in the SB interface region are separated by the strong electric field there, and then decrease the electron−hole recombination rates and increase the carrier lifetime, which result in an increased free carrier density. And the photocurrent decays more rapidly because oxygen is only required to be readsorbed to the interface to modify the interfacial injection (4, 26). We believe that the whole ZnO nanorod and the SB at the metal/ZnO interface both contribute to the photo response characteristics simultaneously. However, the SB plays a more important role in the electrical transport performance of the MSM structural device with Ni electrode than that with Sn electrode, because of the higher SB at the Ni/ZnO interface. And this mechanism also can explain the reason for the larger UV photo response and more rapid decay of ZnO nanorod PD with Ni electrode.

Figure 7 shows the time-resolved photocurrent of a PMMA coated ZnO nanorod PDs in response to the turn-on

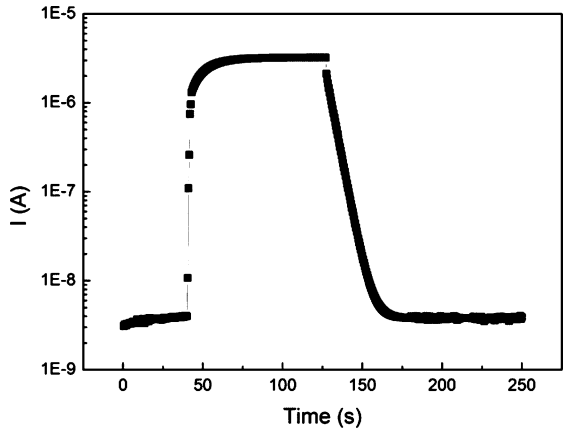

FIGURE 7. UV response time performance of the ZnO nanorods with PMMA coating.

and turn-off of 0.11 mW/cm^2 UV illumination ($\lambda = 365$ nm). The PMMA layer itself contributes nothing to UV response because it is UV transparent and electrically insulating. We can find out that the response speed of the device has been enhanced much with the surface coating of PMMA. It has long been reported that the surface coating of some polymer can improve the UV response speed of ZnO nanostructures (25, 27, 28). Previous literature reports have proposed that coating ZnO with polymers not only prevents the interaction of gases but also passivates the electron states of metal oxides associated to dangling bonds at the surface (25, 27, 28). Therefore, the UV response was dominated by the photogenerated electron−hole pairs, which result in a much faster recombination and decay.

Until now, there have been many reports about ZnO MSM UV PDs. Generally, UV MSM PDs with ZnO nanostructures show higher photoresponse compared to the traditional ZnO film MSM PD, which can be attributed to the large surface-to-volume ratios of ZnO nanostructures easily accelerating oxygen adsorption and desorption at the surface (9, 18, 29). To compare with others reported in the literature, we should compare the key performance parameters, such as responsivity and UV/visible rejection ratio. And we find out that our parameters are better than those reported in majority literatures (9, 18, 30, 31). For example, Ji et al. reported a UV MSM PD with selectively perpendicular grown ZnO nanorod arrays, which shows a responsivity of 41.22 A/W at 5 V bias with 370 nm illumination and a UV/visible rejection ratio of 336.65 (9, 18). Considering the bias voltage, these values are much smaller than those of our sample. We believe it must be attributed to the Schottky contact at the interface and the lateral grown ZnO nanorods, which can be exposed to UV illumination more sufficiently compared with perpendicular grown ZnO nanorods. However, oxygen adsorption is a double-edge sword, and it is responsible for the long recovery time, which also takes place in our experiment. Usually, for ZnO nanostructure MSM UV PDs, especially nanorods grown by hydrothermal approach, a long recovery time ranging from a few minutes to several hours is commonly observed (3, 9, 18, 25). In our experiment, by introducing a relative larger Schottky barrier and a passivation layer, the recovery time can be reduced to a few seconds. This value is comparable with most reports. Therefore, considering the expense and difficulty of technique, we believe our solution is a relatively effective way to fabricate ZnO UV PDs.

4. CONCLUSION

In conclusion, our UV PDs composed of lateral grown ZnO nanorod arrays provides a simple and cost-effective way to fabricate high-performance UV detectors at a low temperature of 90 °C. With the combined effect from a ZnO seed layer and a passivation layer for nanorod growth, ZnO nanorods could only grow laterally between the interdigitated electrodes. The ZnO nanorod devices are visible-blind and have great response even in mid UV region. ZnO nanorod PDs with different metal contact have been fabricated and measured. And the ZnO nanorod PDs with Ni electrode show better performance both in the aspect of photocurrent and response time. We believe it must be attributed to the relative larger Schottky barrier at the Ni/ZnO interface. By surface coating with PMMA, the response has been further improved. Our results imply that ZnO nanorods synthesized by hydrothermal approach are promising candidates for UV detection application.

Acknowledgment. This work was partially supported by the Special Fund of Ministry of Education for Doctor's Conferment Post (20070486015) and the National High Technology Research and Development Program of China (2009AA03Z219).

REFERENCES AND NOTES

(1) Bagnall, D. M.; Zhu, Y. F.; Yao, T.; Koyama, S.; Shen, M. Y.; Goto, T. *Appl. Phys. Lett.* **1997**, *70*, 2230–2232.
(2) Look, D. C.; Reynolds, D. C.; Litton, C. W.; Jones, R. L.; Eason, D. B.; Gantwell, G. *Appl. Phys. Lett.* **2002**, *81*, 1830–1832.
(3) Soci, C.; Zhang, A.; Xiang, B.; Dayeh, S. A.; Aplin, D. P. R.; Park, J.; Bao, X. Y.; Lo, Y. H.; Wang, D. *Nano Lett.* **2007**, *7*, 1003–1009.
(4) Zhou, J.; Gu, Y.; Hu, Y.; Mai, W.; Yeh, P.; Bao, G.; Sood, A. K.; Polla, D. L.; Wang, Z. L. *Appl. Phys. Lett.* **2009**, *94*, 191103.
(5) Islam, M. S.; Sharma, S.; Kamins, T. I.; Williams, R. S. *Nanotechnology* **2004**, *15*, L5–L8.
(6) Chen, R. S.; Wang, S. W.; Lan, Z. H.; Tsai, J. T. H.; Wu, C. T.; Chen, L. C.; Chen, K. H.; Huang, Y. S.; Chen, C. C. *Small* **2008**, *4*, 925–929.
(7) He, R.; Gao, D.; Fan, R.; Hochbaum, A. I.; Carraro, C.; Maboudian, R.; Yang, P. D. *Adv. Mater.* **2005**, *17*, 2098–2102.
(8) Li, Y.; Valle, F. D.; Simonnet, M.; Yamada, I.; Delaunay, J. J. *Nanotechnology* **2009**, *20*, 045501.
(9) Ji, L. W.; Peng, S. M.; Su, Y. K.; Young, S. J.; Wu, C. Z.; Cheng, W. B. *Appl. Phys. Lett.* **2009**, *94*, 203106.
(10) Xu, S.; Ding, Y.; Wei, Y.; Fang, H.; Shen, Y.; Sood, A. K.; Polla, D. L.; Wang, Z. L. *J. Am. Chem. Soc.* **2009**, *131*, 6670–6671.
(11) Qin, Y.; Yang, R. S.; Wang, Z. L. *J. Phys. Chem. C* **2008**, *112*, 18734–18736.
(12) Liu, N. S.; Fang, G. J.; Zeng, W.; Long, H.; Yuan, L. Y.; Zhao, X. Z. *Appl. Phys. Lett.* **2009**, *95*, 153505.
(13) Liu, N. S.; Fang, G. J.; Zeng, W.; Long, H.; Fan, X.; Yuan, L. Y.; Zou, X.; Liu, Y. P.; Zhao, X. Z. *J. Phys. Chem. C* **2010**, *114*, 8575–8580.
(14) Van, D. A.; Meulenkamp, E. A. *J. Lumin.* **2000**, *454*, 87–89.
(15) Vanheusden, K.; Warren, W. L.; Seager, C. H.; Tallant, D. R.; Voigt, J. A.; Gnada, B. E. *J. Appl. Phys.* **1996**, *79*, 7983–7990.
(16) Zhang, X. T.; Liu, Y. C.; Zhang, J. Y.; Lu, Y. M.; Shen, D. Z.; Fan, X. W.; Kong, X. G. *J. Cryst. Growth* **2003**, *254*, 80–85.
(17) Izaki, M.; Watase, S.; Takahashi, H. *Appl. Phys. Lett.* **2003**, *83*, 4930–4932.
(18) Su, Y. K.; Peng, S. M.; Ji, L. W.; Wu, C. Z.; Cheng, W. B.; Liu, C. H. *Langmuir* **2010**, *26*, 603–606.

(19) Zhang, Z. Y.; Jin, C. H.; Liang, X. L.; Chen, Q.; Peng, L. M. *Appl. Phys. Lett.* **2006**, *88*, 073102(3pp).
(20) Zhang, Z. Y.; Yao, K.; Liu, Y.; Jin, C.; Liang, X.; Chen, Q.; Peng, L. M. *Adv. Funct. Mater.* **2007**, *17*, 2478–2489.
(21) Sze, S. M. *Physics of Semiconductor Devices*; Wiley & Sons: New York, 1981.
(22) Zhou, J.; Gu, Y. D.; Fei, P.; Mai, W. J.; Gao, Y. F.; Yang, R. S.; Bao, G.; Wang, Z. L. *Nano Lett.* **2008**, *8*, 3035–3040.
(23) Li, Q.; Gao, T.; Wang, Y. G.; Wang, T. H. *Appl. Phys. Lett.* **2006**, *86*, 123117(3pp).
(24) Reemts, J.; Kittel, A. *J. Appl. Phys.* **2007**, *101*, 013709.
(25) Prades, J. D.; Ramirez, F. H.; Diaz, R. J.; Manzanares, M.; Andreu, T.; Cirera, A.; Rodriguez, A. R.; Morante, J. R. *Nanotechnology* **2008**, *19*, 465501.
(26) Jin, Y.; Wang, J.; Sun, B.; Blakesley, J. C.; Greenham, N. C. *Nano Lett.* **2008**, *8*, 1649–1653.
(27) Park, W. I.; Kim, J. S.; Yi, G.; Bae, M. H.; Lee, H. J. *Appl. Phys. Lett.* **2004**, *85*, 5052–5054.
(28) He, J. H.; Lin, Y. H.; McConney, M. E.; Tsukruk, V. V.; Wang, Z. L.; Bao, G. *J. Appl. Phys.* **2007**, *102*, 084303.
(29) Zhao, Y. M.; Zhang, J. Y.; Jiang, D. Y.; Shan, C. X.; Zhang, Z. Z.; Yao, B.; Zhao, D. X.; Shen, D. Z. *ACS Appl. Mater. Interfaces* **2009**, *1*, 2428–2430.
(30) Weng, W. Y.; Hsueh, T. J.; Chang, S. J.; Chang, S. P.; Hsu, C. L. *Superlattices Microstruct.* **2009**, *46*, 797–802.
(31) Chen, K. J.; Hung, F. Y.; Chang, S. J.; Young, S. J. *J. Alloys Compd.* **2009**, *479*, 674–677.

AM100277Q